

Online: ISSN 2008-949X

Journal of Mathematics and Computer Science



Journal Homepage: www.isr-publications.com/jmcs

Adaptive predefined-time fractional terminal sliding mode control for robotic dynamic systems



Saim Ahmed^{a,b,*}, Ahmad Taher Azar^{a,b}, Walid El-Shafai^{a,b,c}

- ^aCollege of Computer and Information Sciences, Prince Sultan University, Riyadh, Saudi Arabia.
- ^bAutomated Systems and Computing Lab (ASCL), Prince Sultan University, Riyadh, Saudi Arabia.
- ^cDepartment of Electronics and Electrical Communications Engineering, Faculty of Electronic Engineering, Menoufia University, Menouf, 32952, Egypt.

Abstract

This study explores adaptive predefined-time fractional-order proportional-derivative terminal sliding mode control (APt-FoSMC) for robotic manipulators dealing with uncertainties and external disturbances. We introduce a new predefined-time proportional-derivative FoSMC control method that uses proportional-derivative control to ensure guaranteed predefined-time convergence and superior tracking performance. This approach also helps to reduce control input chattering, which is a common issue. The APtFoSMC is designed not to require previous knowledge of the boundaries of the uncertain system dynamics it estimates. Applying the Lyapunov theorem establishes the predefined-time stability of the suggested closed-loop system. We then use computer simulations on a PUMA 560 robotic manipulator system to validate the effectiveness of the suggested APtFoSMC approach.

Keywords: Predefined-time control, fractional SMC scheme, adaptive control, robotic manipulator.

2020 MSC: 93C10, 93D20, 93B52, 93C95.

©2026 All rights reserved.

1. Introduction

Accurate control of robotic manipulators is necessary for automation in a variety of industries. However, it could be challenging to accomplish this control due to their intricate and erratic movements. It is well known that unknown disturbances and uncertainties easily destroy the precision of motion and stability of performance that a manipulation task requires [12]. Most control techniques developed to date rely on a mathematical model of the robot to simulate its behavior and derive a control law [21]. Unfortunately, real robots may behave quite differently due to manufacturing variances. This may result in unexpected behavior or unmodeled dynamics, which can greatly affect control performance and lead to errors, instability, or safety issues [24]. This uncertainty illustrates the increasing need for robotics to develop robust control approaches. Unlike more traditional methods, robust control aims at maintaining desired performance and stability in the presence of these unknowns [3].

Email addresses: sahmed@psu.edu.sa (Saim Ahmed), aazar@psu.edu.sa (Ahmad Taher Azar), welshafai@psu.edu.sa (Walid El-Shafai)

doi: 10.22436/jmcs.041.04.06

Received: 2024-12-15 Revised: 2025-08-27 Accepted: 2025-10-02

^{*}Corresponding author

Because sliding mode control (SMC) can handle external disturbances and uncertainties, it has become increasingly popular for controlling complex systems in recent years. This becomes particularly important for real-world robots with complex dynamics that are difficult to characterize sufficiently [25, 36]. Then, terminal SMC (TSM) was developed, and its advantage was that it guaranteed the state's convergence in a specified period [9, 42]. When robots follow a predetermined path, they are more precise and robust. As stated by this research, TSM may have a larger convergence rate than other approaches [10, 16, 32]. Moreover, some applications of TSM have to be judiciously considered and could pose problems in the long term [11, 31, 35, 38]. The present research is dedicated to making TSM more robust and sensitive [13, 40]. Fractional-order calculus generalizes conventional calculus by permitting integrals and derivatives of arbitrary (non-integer) order; therefore, a subset of generalized differential order is called fractional order [6]. This freedom gives more effective modeling and control in complex systems of science and engineering [18, 20]. According to [28], the FOSMC method is viable for improving robotic system control. FOSMC extends the advantages of conventional sliding mode control by integrating fractionalorder calculus, which can improve tracking and robustness performances against uncertain dynamics [23]. This technique has already been successfully tried with a lot of robotic systems, including autonomous vehicles, mobile robots, and robot manipulators, and that shows potential for better performance in the area of robotic technology [33].

Although finite-time control methods provide guaranteed state convergence in a finite amount of time, the system's initial conditions may affect the actual speed [2]. By guaranteeing convergence within a specified time limit irrespective of the initial state, Fixed-time Sliding Mode Control (FT-SMC) removes this reliance [41]. However, the actual settling time for the actual systems may sometimes be equal to this predefined bound. Moreover, since some systems rely on design characteristics, achieving the planned performance based on this bound can be time-consuming and require lots of effort. The predefined-time control strategy has been devised to improve the control of convergence and get around these restrictions [30]. This approach is more flexible and can offer faster convergence than fixed-time approaches, allowing the designer to designate a desired settling time bound in advance. Consequently, a number of predefined time control schemes have been developed for nonlinear systems. For example, Xue et al. [37] investigate the predefined-time synchronization of multi-input-multi-output chaotic systems and present a novel scheme based on fast TSM controllers and predefined time convergence parameters. Another example is the work by Yang et al. [26], who introduce a novel sigmoid function-based sliding surface design that guarantees robust predefined-time convergence for second-order nonlinear systems with matched disturbances. They establish stability properties through the Lyapunov theorem and propose a robust controller for robotic manipulators to track a predefined contour within a set time, demonstrating precise predefined-time contour tracking without requiring exact knowledge of robot parameters [27].

Since SMC offers a robust approach to controlling systems with known dynamics, its effectiveness can be diminished when systems are subject to unknown dynamics or external disturbances. Adaptive control schemes have emerged as a powerful tool to address these uncertainties. Adaptive control can dynamically adjust to these external influences and system variations, thereby mitigating their impact and improving closed-loop tracking performance [7, 22, 34]. This characteristic has made it a prominent choice for robotic applications. Several researchers have explored and successfully implemented various adaptive control algorithms for a wide range of robotic systems [1, 14, 15, 17]. These studies showcase the effectiveness of this integrated approach in diverse systems, including robotic manipulators, spacecraft, lower-limb exoskeletons, and wind turbines.

This research investigates predefined-time convergence control for robotic manipulators subject to uncertainties and disturbances. We propose a novel adaptive predefined-time fractional-order proportional-derivative sliding mode control (APtFoSMC) scheme. The proposed APtFoSMC offers following. 1. Combining predefined-time SMC with fractional order ensures accurate trajectory tracking and improved closed-loop system response. 2. An adaptive strategy within the PtFoSMC framework tackles unknown dynamics and disturbances, enhancing overall system robustness. 3. Lyapunov stability analysis guarantees predefined-time convergence of the closed-loop system.

The remaining portion of the paper is structured as follows. The preliminaries are given in Section 2. Section 3 covers the robot model and its dynamics. The control design PtFoSMC, APtFoSMC, and their stability investigations using Lyapunov theory are given in Sections 4 and 5, respectively. Section 6 provides simulations to verify our approach. Section 7 expresses discussion and analysis, and Section 8 summarizes the work.

2. Preliminaries

The important preliminaries are given in this section.

Lemma 2.1 ([27]). The predefined stability is computed for the Lyapunov function $\mathcal{L}(t)$ with an initial condition $\mathcal{L}(0)$, as $\dot{\mathcal{L}}(t) \leqslant -\beta_1 \mathcal{L}(t)^{1+\frac{\eta}{2}} - \beta_2 \mathcal{L}(t)^{1-\frac{\eta}{2}}$, where $\beta_i > 0$ and $0 < \eta < 1$. The predefined-time T is formulated as

$$T = \frac{\pi}{\eta \sqrt{\beta_1 \beta_2}}.$$

Lemma 2.2 ([3]). The key inequalities for χ_i can be presented as follows

$$\sum_{i=1}^n \left|\chi_i\right|^{1+\eta} \geqslant \left(\sum_{i=1}^n \left|\chi_i\right|^2\right)^{\frac{1+\eta}{2}}, \text{ when } 0 < \eta < 1, \qquad \sum_{i=1}^n \left|\chi_i\right|^{\eta} \geqslant n^{1-\eta} \left(\sum_{i=1}^n \left|\chi_i\right|\right)^{\eta}, \text{ when } \eta > 1.$$

Definition 2.3. The Riemann-Liouville definition is often utilized in fractional calculus, which defines fractional-order derivatives and integrals as follows [19, 29]:

$${}_{b}\mathfrak{I}^{\bar{\gamma}}_{t}h(t) = \frac{1}{\Gamma(\bar{\gamma})}\int_{b}^{t}\frac{h(\mathfrak{I})}{(t-\mathfrak{I})^{1-\bar{\gamma}}}d\mathfrak{I}, \quad {}_{\lfloor}\mathfrak{D}^{\bar{\bigcirc}}_{\sqcup}\langle(\sqcup) = \frac{\lceil\bar{\bigcirc}\langle(\sqcup)}{\lceil\sqcup\bar{\bigcirc}} = \frac{\infty}{-(\infty-\bar{\bigcirc})}\frac{\lceil}{\lceil\sqcup}\int_{-}^{\sqcup}\frac{\langle(\mathfrak{I})}{(\sqcup-\mathfrak{I})^{\bar{\bigcirc}}}\lceil\mathfrak{I},$$

where $q-1 < \bar{\gamma} < q$, $q \in \mathbb{N}$ and $\Gamma(\cdot)$ is Gamma function, and this is given as $\Gamma(\bar{\gamma}) = \int_0^\infty e^{-t} t^{\bar{\gamma}-1} dt$, where $\mathfrak{I}^{\bar{\gamma}}$ is the fractional-order integral and $\mathfrak{D}^{\bar{\gamma}}$ is the fractional-order derivative of h(t).

Definition 2.4. The fractional-order derivative ${}_b\mathfrak{D}_t^{\bar{\gamma}}h(t)=\frac{1}{\Gamma(1-\bar{\gamma})}\frac{d}{dt}\int_b^t\frac{h(\tau)}{(t-\mathfrak{I})^{\bar{\gamma}}}d\mathfrak{I}$ with $h(t)\in\mathcal{R},0\leqslant\bar{\gamma}<1$, then we can have [39]:

$${}_b\mathfrak{D}_t^{\tilde{\gamma}}sign(h(t))\left\{\begin{array}{ll} >0, & \text{when } h(t)>0 \text{ and } t>0,\\ <0, & \text{when } h(t)<0 \text{ and } t>0. \end{array}\right.$$

3. Robot dynamics

The model presented herein describes the dynamic equation of the robotic manipulator utilized in this study [3]:

$$\mathfrak{M}(\mathbf{x})\ddot{\mathbf{x}} + \mathfrak{C}(\mathbf{x}, \dot{\mathbf{x}})\dot{\mathbf{x}} + \mathfrak{G}(\mathbf{x}) = \mathbf{u}(\mathbf{t}) + \mathbf{u}_{\mathbf{d}}(\mathbf{t}) + \mathbf{u}_{\mathbf{f}}(\mathbf{t}), \tag{3.1}$$

where $x \in \mathbb{R}^n$, $\dot{x} \in \mathbb{R}^n$, and $\ddot{x} \in \mathbb{R}^n$ are angular position, velocity, and acceleration, respectively. $\mathfrak{M}(x) \in \mathbb{R}^{n \times n} > 0$ symbolizes inertia matrix with $0 < \check{x}_1(\mathfrak{M}(x)) \leqslant \|\mathfrak{M}(x)\| \leqslant \check{x}_2(\mathfrak{M}(x))$, where \check{x}_1 and \check{x}_2 are the small and large eigenvalues of matrix $\mathfrak{M}(x)$, respectively. $\mathfrak{C}(x,\dot{x}) \in \mathbb{R}^{n \times n}$ is the coriolis and centripetal forces, and $\mathfrak{G}(x) \in \mathbb{R}^n$ represents the gravitational force. Moreover, $\mathfrak{u}_f(t) \in \mathbb{R}^n$ are uncertain dynamics. $\mathfrak{u}(t) \in \mathbb{R}^n$ is the control torque input, and $\mathfrak{u}_d(t) \in \mathbb{R}^n$ is the unknown external disturbances. Equation (3.1), as mentioned above, is provided as follows:

$$\mathcal{M}(\mathbf{x})\ddot{\mathbf{x}} = \mathbf{u}(\mathbf{t}) + \mathbf{u}_{\mathbf{d}}(\mathbf{t}) + \mathbf{u}_{\mathbf{f}}(\mathbf{t}) - \mathcal{C}(\mathbf{x}, \dot{\mathbf{x}})\dot{\mathbf{x}} - \mathcal{G}(\mathbf{x}), \quad \ddot{\mathbf{x}} = \mathcal{M}^{-1}(\mathbf{x})(\mathbf{u}(\mathbf{t}) + \mathbf{u}_{\mathbf{d}}(\mathbf{t}) + \mathbf{u}_{\mathbf{f}}(\mathbf{t}) - \mathcal{C}(\mathbf{x}, \dot{\mathbf{x}})\dot{\mathbf{x}} - \mathcal{G}(\mathbf{x})).$$

The definition of the tracking error is as follows:

$$\dot{\varepsilon}_2 = \mathcal{M}^{-1}(x)(u(t) + u_d(t) + u_f(t) - \mathcal{C}(x, \dot{x})\dot{x} - \mathcal{G}(x)) - \ddot{x}_d, \tag{3.2}$$

where $\varepsilon_1 = x - x_d$, $\dot{\varepsilon}_1 = \varepsilon_2$ is tracking error, and x_d is desired reference input.

4. PtFoSMC design

In this section, a novel control strategy for robotic manipulators subjected to exogenous disturbances and uncertainty is developed. First, the main features of the proposed predefined-time fractional-order proportional-derivative sliding mode control (PtFoSMC) are reviewed.

4.1. Predefined-time fractional-order sliding surface design

Inspired by SMC's intrinsic fast convergence and robustness, researchers have explored various sliding surfaces to enhance control performance. In this case, the proposed sliding surface's ability to provide accurate and fast predefined-time control for n-DOF robotic manipulators will make it even more desirable. Therefore, driven by the above discussion, the fractional-order-based proposed sliding surface is devised as

$$\zeta(t) = \kappa_1 |\varepsilon_1|^{1 + \frac{\alpha}{2}} \operatorname{sign}(\varepsilon_1) + \kappa_2 |\varepsilon_1|^{1 - \frac{\alpha}{2}} \operatorname{sign}(\varepsilon_1) + \kappa_3 \mathfrak{D}^{\gamma} \operatorname{sign}(\varepsilon_1) + \kappa_4 \varepsilon_2, \tag{4.1}$$

where $\zeta(t) \in \mathbb{R}^n$ denotes the sliding variable, $\kappa_1, \kappa_2, \kappa_3, \kappa_4 \in \mathbb{R}^+$, and $0 < \alpha, \gamma < 1$. Afterwards, $\dot{\zeta}(t)$ can be calculated as

$$\dot{\zeta}(t) = \kappa_1 (1 + \frac{\alpha}{2}) |\epsilon_1|^{\frac{\alpha}{2}} \epsilon_2 + \kappa_2 (1 - \frac{\alpha}{2}) |\epsilon_1|^{-\frac{\alpha}{2}} \epsilon_2 + \kappa_3 \mathfrak{D}^{\gamma + 1} sign(\epsilon_1) + \kappa_4 \dot{\epsilon}_2. \tag{4.2}$$

The substitution of (3.2) into (4.2) yields

$$\begin{split} \dot{\zeta}(t) &= \kappa_{1}(1+\frac{\alpha}{2})|\epsilon_{1}|^{\frac{\alpha}{2}}\epsilon_{2} + \kappa_{2}(1-\frac{\alpha}{2})|\epsilon_{1}|^{-\frac{\alpha}{2}}\epsilon_{2} + \kappa_{3}\mathfrak{D}^{\gamma+1}sign(\epsilon_{1}) \\ &+ \kappa_{4}\left(\mathfrak{M}^{-1}(x)(\mathfrak{u}(t)+\mathfrak{u}_{d}(t)+\mathfrak{u}_{f}(t)-\mathfrak{C}(x,\dot{x})\dot{x}-\mathfrak{G}(x))-\ddot{x}_{d}\right). \end{split} \tag{4.3}$$

We can express equation (4.3) as

$$\begin{split} \dot{\zeta}(t) &= \kappa_{1}(1+\frac{\alpha}{2})|\epsilon_{1}|^{\frac{\alpha}{2}}\epsilon_{2} + \kappa_{2}(1-\frac{\alpha}{2})|\epsilon_{1}|^{-\frac{\alpha}{2}}\epsilon_{2} + \kappa_{3}\mathfrak{D}^{\gamma+1}\text{sign}(\epsilon_{1}) \\ &+ \kappa_{4}\left(\mathfrak{M}^{-1}(x)(\mathfrak{u}(t) - \mathfrak{C}(x,\dot{x})\dot{x} - \mathfrak{G}(x)) + \mathfrak{O}(x,\dot{x},\ddot{x}) - \ddot{x}_{d}\right), \end{split} \tag{4.4}$$

where $\mathcal{O}(x,\dot{x},\ddot{x})=\mathcal{M}^{-1}(x)(\mathfrak{u}_f(t)+\mathfrak{u}_d(t))$. We now design the PtFoSMC method for n-DOF robotic manipulators using the provided sliding surface. This control law is designed to be robust against unknown disturbances and uncertainties.

Assumption 4.1. The bounds of the unknown uncertainties and external disturbances affecting the dynamical system are expressed under equation (4.5):

$$\|\mathcal{O}(x,\dot{x},\ddot{x})\| \leqslant \mathcal{O}_1 + \mathcal{O}_2 \|x\| + \mathcal{O}_3 \|\dot{x}\|^2,\tag{4.5}$$

where O_1 , O_2 , and O_3 are unknown positive constants.

4.2. PtFoSMC control design

The PtFoSMC control law is created in the following way to ensure that robotic manipulators operate reliably in the face of external disturbances and bounded uncertainties:

$$u(t) = \mathfrak{M}(x) \left(\begin{array}{l} \mathfrak{M}^{-1}(x) C(x, \dot{x}) \dot{x} + \mathfrak{M}^{-1}(x) G(x) + \ddot{x}_d - (\mathfrak{O}_1 + \mathfrak{O}_2 \|x\| + \mathfrak{O}_3 \|\dot{x}\|^2) sign(\zeta(t)) \\ - \kappa_4^{-1} \kappa_1 (1 + \frac{\alpha}{2}) |\epsilon_1|^{\frac{\alpha}{2}} \epsilon_2 - \kappa_4^{-1} \kappa_2 (1 - \frac{\alpha}{2}) |\epsilon_1|^{-\frac{\alpha}{2}} \epsilon_2 - \kappa_4^{-1} \kappa_3 \mathfrak{D}^{\gamma + 1} sign(\epsilon_1) \\ - \kappa_4^{-1} \kappa_5 |\zeta(t)|^{1 + \frac{\beta}{2}} sign(\zeta(t)) - \kappa_4^{-1} \kappa_6 |\zeta(t)|^{1 - \frac{\beta}{2}} sign(\zeta(t)) - \kappa_4^{-1} \kappa_7 \mathfrak{D}^{\gamma} sign(\zeta(t)) \end{array} \right), \quad (4.6)$$

where $|\epsilon|^{-\frac{\alpha}{2}}=0$ if $\epsilon=0$, κ_5 , κ_6 , κ_7 are positive constants, and β is constant satisfying $0<\beta<1$. By substituting $\mathfrak{u}(t)$ into (4.4), $\dot{\zeta}(t)$ can be computed as

$$\dot{\zeta}(t) = \kappa_{1}(1+\frac{\alpha}{2})|\epsilon_{1}|^{\frac{\alpha}{2}}\epsilon_{2} + \kappa_{2}(1-\frac{\alpha}{2})|\epsilon_{1}|^{-\frac{\alpha}{2}}\epsilon_{2} + \kappa_{3}\mathfrak{D}^{\gamma+1}sign(\epsilon_{1})$$

$$+ \kappa_{4} \left(\begin{array}{c} \mathcal{M}^{-1}(x)\mathcal{C}(x,\dot{x})\dot{x} + \mathcal{M}^{-1}(x)\mathcal{G}(x) + \ddot{x}_{d} \\ -(\mathcal{O}_{1}+\mathcal{O}_{2}\|x\|+\mathcal{O}_{3}\|\dot{x}\|^{2})sign(\zeta(t)) \\ -\kappa_{4}^{-1}\kappa_{1}(1+\frac{\alpha}{2})|\epsilon_{1}|^{\frac{\alpha}{2}}\epsilon_{2} - \kappa_{4}^{-1}\kappa_{2}(1-\frac{\alpha}{2})|\epsilon_{1}|^{-\frac{\alpha}{2}}\epsilon_{2} \\ -\kappa_{4}^{-1}\kappa_{3}\mathfrak{D}^{\gamma+1}sign(\epsilon_{1}) \\ -\kappa_{4}^{-1}\kappa_{5}|\zeta(t)|^{1+\frac{\beta}{2}}sign(\zeta(t)) - \kappa_{4}^{-1}\kappa_{6}|\zeta(t)|^{1-\frac{\beta}{2}}sign(\zeta(t)) \\ -\mathcal{M}^{-1}(x)\mathcal{C}(x,\dot{x})\dot{x} - \mathcal{M}^{-1}(x)\mathcal{G}(x)) + \mathcal{O}(x,\dot{x},\ddot{x}) - \ddot{x}_{d} \end{array} \right)$$

Simplification of (4.7), $\dot{\zeta}(t)$ can be obtained as

$$\begin{split} \dot{\zeta}(t) &= -\kappa_4(\mathcal{O}_1 + \mathcal{O}_2 \|\mathbf{x}\| + \mathcal{O}_3 \|\dot{\mathbf{x}}\|^2) sign(\zeta(t)) + \kappa_4 \mathcal{O}(\mathbf{x}, \dot{\mathbf{x}}, \ddot{\mathbf{x}}) \\ &- \kappa_5 |\zeta(t)|^{1 + \frac{\beta}{2}} sign(\zeta(t)) - \kappa_6 |\zeta(t)|^{1 - \frac{\beta}{2}} sign(\zeta(t)) - \kappa_7 \mathfrak{D}^{\gamma} sign(\zeta(t)). \end{split} \tag{4.8}$$

The control scheme and sliding surface have been designed, and we will proceed with the stability analyses.

4.3. Stability analyses

An analysis of the stability of the closed-loop system is conducted in this section, utilizing the Lyapunov theorem. Equation (3.1) is employed to represent the system dynamics. When $\zeta(t) = 0$ from (4.1), we can have

$$\varepsilon_{2} = -\kappa_{1}/\kappa_{4}|\varepsilon_{1}|^{1+\frac{\alpha}{2}}\operatorname{sign}(\varepsilon_{1}) - \kappa_{2}/\kappa_{4}|\varepsilon_{1}|^{1-\frac{\alpha}{2}}\operatorname{sign}(\varepsilon_{1}) - \kappa_{3}/\kappa_{4}\mathfrak{D}^{\gamma}\operatorname{sign}(\varepsilon_{1}). \tag{4.9}$$

To establish the stability of the tracking error, we carefully select a Lyapunov function candidate as follows:

$$L_{\varepsilon}(t) = \frac{1}{2} \sum_{i=1}^{n} \varepsilon_{1i}^{2}(t). \tag{4.10}$$

The derivative of (4.10) is computed, and it can be expressed as

$$\dot{\mathsf{L}}_{\varepsilon}(\mathsf{t}) = \sum_{i=1}^{n} \varepsilon_{1i}(\mathsf{t})\varepsilon_{2i}(\mathsf{t}). \tag{4.11}$$

By substituting equation (4.9) into equation (4.11), we can obtain

$$\dot{L}_{\epsilon}(t) = \sum_{i=1}^{n} \epsilon_{1i}(t) \left(-\kappa_{1}/\kappa_{4}|\epsilon_{1}|^{1+\frac{\alpha}{2}} sign(\epsilon_{1}) - \kappa_{2}/\kappa_{4}|\epsilon_{1}|^{1-\frac{\alpha}{2}} sign(\epsilon_{1}) - \kappa_{3}/\kappa_{4} \mathfrak{D}^{\gamma} sign(\epsilon_{1}) \right).$$

Following simplification using Definition 2.4, the equation transforms into:

$$\dot{L}_{\epsilon}(t) \leqslant -\kappa_1/\kappa_4 \sum_{i=1}^n \left(|\epsilon_{1i}(t)|^2 \right)^{\frac{4+\alpha}{4}} - \kappa_2/\kappa_4 \sum_{i=1}^n \left(|\epsilon_{1i}(t)|^2 \right)^{\frac{4-\alpha}{4}}.$$

By utilizing Lemma 2.2, we can express the above equation more concisely.

$$\dot{L}_\epsilon(t) \leqslant -\kappa_1/\kappa_4 n^{-\frac{\alpha}{4}} \Biggl(\sum_{i=1}^n |\epsilon_{1i}(t)|^2 \Biggr)^{\frac{4+\alpha}{4}} - \kappa_2/\kappa_4 \Biggl(\sum_{i=1}^n |\epsilon_{1i}(t)|^2 \Biggr)^{\frac{4-\alpha}{4}}.$$

It can be represented as

$$\dot{L}_{\epsilon}(t)\leqslant -\kappa_{1}/\kappa_{4}2^{\frac{4+\alpha}{4}}n^{-\frac{\alpha}{4}}L_{\epsilon}^{\frac{4+\alpha}{4}}-\kappa_{2}/\kappa_{4}2^{\frac{4-\alpha}{4}}L_{\epsilon}^{\frac{4-\alpha}{4}}=-\kappa_{1}/\kappa_{4}2^{1+\frac{\alpha}{4}}n^{-\frac{\alpha}{4}}L_{\epsilon}^{1+\frac{\alpha}{4}}-\kappa_{2}/\kappa_{4}2^{1-\frac{\alpha}{4}}L_{\epsilon}^{1-\frac{\alpha}{4}}.$$

By applying Lemma 2.1, we can illustrate that the sliding surface, as defined in equation (4.1), converges to zero within a predetermined time frame

$$\mathsf{T}_{\epsilon} = \frac{2\pi}{\alpha\sqrt{2^{1+\frac{\alpha}{4}}2^{1-\frac{\alpha}{4}}n^{-\frac{\alpha}{4}}\kappa_{1}\kappa_{2}/\kappa_{4}^{2}}} = \frac{\pi}{\alpha\sqrt{\kappa_{1}\kappa_{2}n^{-\frac{\alpha}{4}}/\kappa_{4}^{2}}}.$$

Theorem 4.2. By employing the model of an n-DOF robotic manipulator (3.1), utilizing the designed sliding surface (4.1), and implementing the PtFoSMC control method (4.6), we can confidently ensure that the system trajectory of the manipulator will converge to zero within a predefined time. This convergence is guaranteed under the condition for bounded uncertainties and disturbances specified in Equation (4.5).

Proof. The Lyapunov function candidate has been chosen as shown below:

$$L_{\zeta}(t) = \frac{1}{2} \sum_{i=1}^{n} \zeta_{i}^{2}(t). \tag{4.12}$$

Taking derivative of (4.12), $\dot{L}_{\zeta}(t)$ can be obtained as follows:

$$\dot{L}_{\zeta}(t) = \sum_{i=1}^{n} \zeta_{i}(t)\dot{\zeta}_{i}(t). \tag{4.13}$$

After substituting equation (4.8) into equation (4.13), we can derive as

$$\dot{L}_{\zeta}(t) = \sum_{i=1}^{n} \zeta_{i}(t) \begin{bmatrix} -\kappa_{4}(\mathcal{O}_{1} + \mathcal{O}_{2} \|\mathbf{x}\| + \mathcal{O}_{3} \|\dot{\mathbf{x}}\|^{2}) sign(\zeta(t)) + \kappa_{4}\mathcal{O}(\mathbf{x}, \dot{\mathbf{x}}, \ddot{\mathbf{x}}) \\ -\kappa_{5} |\zeta(t)|^{1+\frac{\beta}{2}} sign(\zeta(t)) - \kappa_{6} |\zeta(t)|^{1-\frac{\beta}{2}} sign(\zeta(t)) - \kappa_{7} \mathfrak{D}^{\gamma} sign(\zeta(t)) \end{bmatrix}. \tag{4.14}$$

We can then solve equation (4.14) based on Assumption 4.1 as

$$\dot{L}_{\zeta}(t)\leqslant \sum_{i=1}^{n}\zeta_{i}(t)\left[-\kappa_{5}|\zeta(t)|^{1+\frac{\beta}{2}}sign(\zeta(t))-\kappa_{6}|\zeta(t)|^{1-\frac{\beta}{2}}sign(\zeta(t))\right].$$

Then it can be expressed as

$$\dot{L}_{\zeta}(t) \leqslant -\kappa_5 \sum_{i=1}^n \left(|\zeta_i(t)|^2 \right)^{\frac{4+\beta}{4}} - \kappa_6 \sum_{i=1}^n \left(|\zeta_i(t)|^2 \right)^{\frac{4-\beta}{4}}.$$

Utilizing Lemma 2.2, we can express the resulting equation

$$\dot{L}_{\zeta}(t) \leqslant -\kappa_{5} n^{-\frac{\beta}{4}} \left(\sum_{i=1}^{n} |\zeta_{i}(t)|^{2} \right)^{\frac{4+\beta}{4}} - \kappa_{6} \left(\sum_{i=1}^{n} |\zeta_{i}(t)|^{2} \right)^{\frac{4-\beta}{4}}. \tag{4.15}$$

And subsequently, equation (4.15) can be obtained as

$$\dot{L}_{\zeta}(t) \leqslant -\kappa_{5} n^{-\frac{\beta}{4}} 2^{\frac{4+\beta}{4}} L_{\zeta}(t)^{\frac{4+\beta}{4}} - \kappa_{6} 2^{\frac{4-\beta}{4}} L_{\zeta}(t)^{\frac{4-\beta}{4}}. \tag{4.16}$$

This analysis validates that the system trajectory converges to the sliding surface $\zeta(t)$ in a predefined time. Lemma 2.1 proves that the following is a mathematical expression for this convergence time:

$$T_{\zeta} = \frac{2\pi}{\beta \sqrt{\kappa_5 \kappa_6 n^{-\frac{\beta}{4}} 2^{1+\frac{\beta}{4}} 2^{1-\frac{\beta}{4}}}} = \frac{\pi}{\beta \sqrt{n^{-\frac{\beta}{4}} \kappa_5 \kappa_6}}.$$
 (4.17)

Now, the total setting time can be estimated considering T_{ϵ} and T_{ζ} to justify the predefined time convergence of the presented methodology and to illustrate its adaptability within PtFoSMC principles.

5. APtFoSMC control design

An effective new APtFoSMC architecture is developed in this section to hold robustness against unknown system dynamics by estimating them. In doing so, this new approach eliminates the problem of unknown system dynamics by proposing an adaptation mechanism for the first time within this framework. The proposed scheme is, therefore, designed to achieve robustness to compensate for unknown dynamics:

$$u(t) = \mathfrak{M}(x) \left(\begin{array}{l} \mathfrak{M}^{-1}(x) \mathfrak{C}(x, \dot{x}) \dot{x} + \mathfrak{M}^{-1}(x) \mathfrak{G}(x) + \ddot{x}_d - (\hat{\mathbb{O}}_1 + \hat{\mathbb{O}}_2 \|x\| + \hat{\mathbb{O}}_3 \|\dot{x}\|^2) sign(\zeta(t)) \\ -\kappa_4^{-1} \kappa_1 (1 + \frac{\alpha}{2}) |\epsilon_1|^{\frac{\alpha}{2}} \epsilon_2 - \kappa_4^{-1} \kappa_2 (1 - \frac{\alpha}{2}) |\epsilon_1|^{-\frac{\alpha}{2}} \epsilon_2 - \kappa_4^{-1} \kappa_3 \mathfrak{D}^{\gamma + 1} sign(\epsilon_1) \\ -\kappa_4^{-1} \kappa_5 |\zeta(t)|^{1 + \frac{\beta}{2}} sign(\zeta(t)) - \kappa_4^{-1} \kappa_6 |\zeta(t)|^{1 - \frac{\beta}{2}} sign(\zeta(t)) - \kappa_4^{-1} \kappa_7 \mathfrak{D}^{\gamma} sign(\zeta(t)) \end{array} \right), \quad (5.1)$$

where $\hat{\mathbb{O}}_1$, $\hat{\mathbb{O}}_2$, and $\hat{\mathbb{O}}_3$ represent the estimates of unknown constants \mathbb{O}_1 , \mathbb{O}_2 , and \mathbb{O}_3 , respectively. Upon substituting $\mathfrak{u}(t)$ (5.1) into (4.4), the expression (5.2) can be formulated as

$$\dot{\zeta}(t) = \kappa_{1}(1 + \frac{\alpha}{2})|\epsilon_{1}|^{\frac{\alpha}{2}}\epsilon_{2} + \kappa_{2}(1 - \frac{\alpha}{2})|\epsilon_{1}|^{-\frac{\alpha}{2}}\epsilon_{2} + \kappa_{3}\mathfrak{D}^{\gamma+1}\mathrm{sign}(\epsilon_{1})$$

$$+ \kappa_{4} \left(\begin{array}{c} \mathcal{M}^{-1}(x)\mathcal{C}(x,\dot{x})\dot{x} + \mathcal{M}^{-1}(x)\mathcal{G}(x) + \ddot{x}_{d} \\ -(\hat{\mathbb{O}}_{1} + \hat{\mathbb{O}}_{2} \|x\| + \hat{\mathbb{O}}_{3} \|\dot{x}\|^{2})\mathrm{sign}(\zeta(t)) \\ -\kappa_{4}^{-1}\kappa_{1}(1 + \frac{\alpha}{2})|\epsilon_{1}|^{\frac{\alpha}{2}}\epsilon_{2} - \kappa_{4}^{-1}\kappa_{2}(1 - \frac{\alpha}{2})|\epsilon_{1}|^{-\frac{\alpha}{2}}\epsilon_{2} \\ -\kappa_{4}^{-1}\kappa_{3}\mathfrak{D}^{\gamma+1}\mathrm{sign}(\epsilon_{1}) \\ -\kappa_{4}^{-1}\kappa_{5}|\zeta(t)|^{1+\frac{\beta}{2}}\mathrm{sign}(\zeta(t)) - \kappa_{4}^{-1}\kappa_{6}|\zeta(t)|^{1-\frac{\beta}{2}}\mathrm{sign}(\zeta(t)) \\ -\mathcal{M}^{-1}(x)\mathcal{C}(x,\dot{x})\dot{x} - \mathcal{M}^{-1}(x)\mathcal{G}(x)) + \mathcal{O}(x,\dot{x},\ddot{x}) - \ddot{x}_{d} \end{array} \right)$$
 (5.2)

Then it can be simplified as

$$\begin{split} \dot{\zeta}(t) &= -\kappa_4(\hat{\mathbb{O}}_1 + \hat{\mathbb{O}}_2 \left\| \boldsymbol{x} \right\| + \hat{\mathbb{O}}_3 \|\dot{\boldsymbol{x}}\|^2) sign(\zeta(t)) + \kappa_4 \mathbb{O}(\boldsymbol{x}, \dot{\boldsymbol{x}}, \ddot{\boldsymbol{x}}) \\ &- \kappa_5 |\zeta(t)|^{1+\frac{\beta}{2}} sign(\zeta(t)) - \kappa_6 |\zeta(t)|^{1-\frac{\beta}{2}} sign(\zeta(t)) - \kappa_7 \mathfrak{D}^{\gamma} sign(\zeta(t)). \end{split} \tag{5.3}$$

Adaptive laws are developed to counteract the uncertain dynamics effectively

$$\dot{\hat{\mathbb{O}}}_{1} = \begin{cases} \kappa_{4} \rho_{i} \|\zeta(t)\| \mathcal{X}, & \text{for } \|\zeta(t)\| > \alpha, \\ 0, & \text{for } \|\zeta(t)\| \leqslant \alpha, \end{cases}$$
 (5.4)

where $\mathfrak{X}=\left[1,\|x\|\,,\|\dot{x}\|^2\right]$, $\alpha>0$, and $\rho_i>0$ are positive constants. The designed block diagram is presented in Figure 1.

APtFoSMC is based on the condition (4.5) for the uncertain manipulator dynamics to be robustly stable. Therefore, this theorem is very important in the proof of stability analysis of any predefined time control scheme.

Theorem 5.1. This theorem establishes the predefined-time stability of the uncertain system (3.1) in the presence of unknown external disturbances. It ensures that the system trajectory converges to the desired equilibrium point within a predefined time frame when utilizing the proposed surface (4.1) and the APtFoSMC control law (5.1) with the adaptive laws defined in (5.4). This convergence is guaranteed under the conditions outlined in Assumption 4.1.

Proof. We appropriately select the Lyapunov function candidate as follows

$$L_{\mathcal{O}}(t) = \frac{1}{2} \sum_{i=1}^{n} \zeta_{i}^{2}(t) + \frac{\Delta \mathcal{O}_{1}^{2}}{2\rho_{1}} + \frac{\Delta \mathcal{O}_{2}^{2}}{2\rho_{2}} + \frac{\Delta \mathcal{O}_{3}^{2}}{2\rho_{3}},$$

where $\Delta \theta_i = \hat{\theta}_i - \theta_i$ represents the adaptive error. To compute the derivative of $L_0(t)$, we can use the following approach:

$$\dot{\mathbf{L}}_{\mathcal{O}}(\mathbf{t}) = \sum_{i=1}^{n} \zeta_{i}(\mathbf{t})\dot{\zeta}_{i}(\mathbf{t}) + \frac{\Delta\mathcal{O}_{1}}{\rho_{1}}\dot{\hat{\mathcal{O}}}_{1} + \frac{\Delta\mathcal{O}_{2}}{\rho_{2}}\dot{\hat{\mathcal{O}}}_{2} + \frac{\Delta\mathcal{O}_{3}}{\rho_{3}}\dot{\hat{\mathcal{O}}}_{3}. \tag{5.5}$$

Substituting the expression for $\dot{\zeta}(t)$ (5.3) into equation (5.5) results in:

$$\begin{split} \dot{L}_{\mathfrak{O}}(t) &= \sum_{i=1}^{n} \zeta_{i}(t) \left[\begin{array}{l} -\kappa_{4}(\hat{\mathbb{O}}_{1} + \hat{\mathbb{O}}_{2} \left\| \boldsymbol{x} \right\| + \hat{\mathbb{O}}_{3} \|\dot{\boldsymbol{x}}\|^{2}) sign(\zeta(t)) + \kappa_{4} \mathbb{O}(\boldsymbol{x}, \dot{\boldsymbol{x}}, \ddot{\boldsymbol{x}}) \\ -\kappa_{5} |\zeta(t)|^{1+\frac{\beta}{2}} sign(\zeta(t)) - \kappa_{6} |\zeta(t)|^{1-\frac{\beta}{2}} sign(\zeta(t)) - \kappa_{7} \mathfrak{D}^{\gamma} sign(\zeta(t)) \\ + \frac{\Delta \mathbb{O}_{1}}{\rho_{1}} \dot{\hat{\mathbb{O}}}_{1} + \frac{\Delta \mathbb{O}_{2}}{\rho_{2}} \dot{\hat{\mathbb{O}}}_{2} + \frac{\Delta \mathbb{O}_{3}}{\rho_{3}} \dot{\hat{\mathbb{O}}}_{3}. \end{array} \right] \end{split}$$

By utilizing equations (5.4), (4.5), and Definition 2.4, we can effectively solve

$$\dot{L}_{\mathfrak{O}}(t) \leqslant -\kappa_{5} \underset{i=1}{\overset{n}{\sum}} \left(|\zeta_{i}(t)|^{2} \right)^{\frac{4+\beta}{4}} - \kappa_{6} \underset{i=1}{\overset{n}{\sum}} \left(|\zeta_{i}(t)|^{2} \right)^{\frac{4-\beta}{4}}.$$

In line with Lemma 2.2, we obtain equation (5.6):

$$\dot{L}_{\mathcal{O}}(t) \leqslant -\kappa_{5} n^{-\frac{\beta}{4}} \left(\sum_{i=1}^{n} |\zeta_{i}(t)|^{2} \right)^{\frac{4+\beta}{4}} - \kappa_{6} \left(\sum_{i=1}^{n} |\zeta_{i}(t)|^{2} \right)^{\frac{4-\beta}{4}}. \tag{5.6}$$

To ascertain the predefined time, we can compute equation (5.7) as follows:

$$\dot{L}_{\mathcal{O}}(t) \leqslant -\kappa_{5} n^{-\frac{\beta}{4}} (2[L_{\mathcal{O}}(t) - \nabla])^{\frac{4+\beta}{4}} - \kappa_{6} (2[L_{\mathcal{O}}(t) - \nabla])^{\frac{4-\beta}{4}}, \tag{5.7}$$

where $\nabla = \frac{\Delta O_1^2}{2\rho_1} + \frac{\Delta O_2^2}{2\rho_2} + \frac{\Delta O_3^2}{2\rho_3}$. It can be rewritten as

$$\begin{split} \dot{L}_{\circlearrowleft}(t) \leqslant & -\kappa_{5} 2^{\frac{4+\beta}{4}} n^{-\frac{\beta}{4}} (L_{\circlearrowleft}(t) - \nabla)^{\frac{4+\beta}{4}} - \kappa_{6} 2^{\frac{4-\beta}{4}} (L_{\circlearrowleft}(t) - \nabla)^{\frac{4-\beta}{4}} \\ \leqslant & -\kappa_{5} 2^{\frac{4+\beta}{4}} n^{-\frac{\beta}{4}} (1 - \frac{\nabla}{L_{\circlearrowleft}(t)})^{\frac{4+\beta}{4}} L_{\circlearrowleft}(t)^{\frac{4+\beta}{4}} - \kappa_{6} 2^{\frac{4-\beta}{4}} (1 - \frac{\nabla}{L_{\circlearrowleft}(t)})^{\frac{4-\beta}{4}} L_{\circlearrowleft}(t)^{\frac{4-\beta}{4}}. \end{split}$$

The following text can now be presented in a simplified form:

$$\dot{L}_{\mathcal{O}}(t) \leqslant -\mho_{1}L_{\mathcal{O}}(t)^{1+\frac{\beta}{4}} - \mho_{2}L_{\mathcal{O}}(t)^{1-\frac{\beta}{4}},$$

where $\mho_1=\kappa_5 2^{\frac{4+\beta}{4}} n^{-\frac{\beta}{4}} (1-\frac{\nabla}{L_{\mathbb{O}}(\mathfrak{t})})^{\frac{4+\beta}{4}}$, $\mho_2=\kappa_6 2^{\frac{4-\beta}{4}} (1-\frac{\nabla}{L_{\mathbb{O}}(\mathfrak{t})})^{\frac{4-\beta}{4}}$. By utilizing Lemma 2.1, we can calculate the predefined time $T_{\mathbb{O}}$, ensuring that the state trajectories converge to zero within this predetermined time frame

$$T_{\text{O}} = \frac{2\pi}{\beta\sqrt{\mho_{1}\mho_{2}}}.$$

Adding T_0 and T_ϵ allows us to calculate the total predefined time convergence, which guarantees precise and swift control performance. For a graphical representation of the complete structure of the proposed APtFoSMC scheme, please see Figure 1.

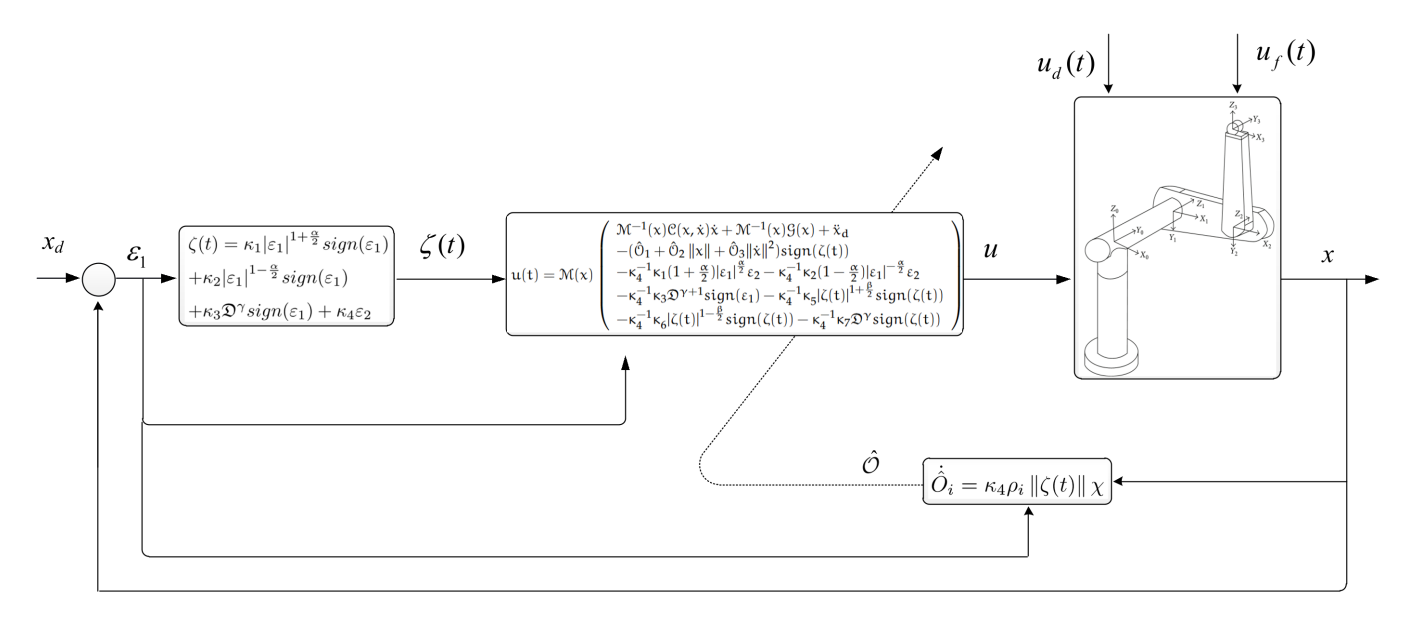


Figure 1: Block diagram of the designed method.

Remark 5.2. When the suggested scheme is implemented on the dynamics of the robotic model (3.1), utilizing the sliding manifold (4.1) and the control law (5.1) updated by the adaptive laws (5.4), it effectively achieves the desired tracking error outcomes $\lim_{t\to T} \varepsilon(t) \to 0$. The subsequent step will involve presenting a numerical simulation to further illustrate these results, which will be explored in the following section.

6. Numerical results

A simulation study assesses the effectiveness of the proposed adaptive predefined-time proportional-derivative terminal sliding mode control (APtFoSMC) scheme applied to the uncertain dynamics of 3-DOF PUMA 560 robot under external disturbances [8]. This study compares the performance of APtFoSMC with the adaptive finite-time terminal SMC (AFtSMC) approach [4] and adaptive time delay estimation high-order SMC (ATDEHSMC) [5] in the presence of external disturbances and uncertainties. The desired trajectories, external disturbances, and uncertain dynamics are described as:

$$\begin{aligned} x_d = \left[\begin{array}{c} \cos(0.2\pi t) - 1 \\ \cos(0.2\pi t + 0.5\pi) \\ \sin(0.2\pi t + 0.5\pi) - 1 \end{array} \right], \quad u_f = \left[\begin{array}{c} 0.5\dot{x}_1 + \sin(3x_1) \\ 1.3\dot{x}_2 - 1.8\sin(2x_2) \\ -0.1\dot{x}_3 - 0.5\sin(x_3) \end{array} \right], \quad u_d = \left[\begin{array}{c} 0.5\sin(\dot{x}_1) \\ 1.1\sin(\dot{x}_2) \\ 0.15\sin(\dot{x}_3) \end{array} \right]. \end{aligned}$$

Following that, a detailed analysis of the dynamics and parameters of the robot has been taken from [8]. Furthermore, the suitable parameters for the developed APtFoSMC scheme are detailed in Table 1.

The simulation results compared, such as angular position tracking, tracking error, control torques, and adaptive parameter estimations of the proposed scheme with the AFtSMC and ATDEHSMC methods applied to the 3-DOF robotic manipulator under unknown uncertain dynamics, are given in Figures 2-5, respectively.

From the numerical simulations in the figures, the proposed APtFoSMC scheme's performance is compared to the AFtSMC and ATDEHSMC controllers under well-defined conditions. This evaluation includes a comprehensive analysis of their performance depicted in Figures 2-5, particularly when handling unknown system dynamics. For a clear comparison in performance, Figures 2-4 depict the APtFoSMC controller's performance under uncertain dynamics with AFtSMC and ATDEHSMC. Figure 2 shows how the controller tracks the desired trajectory precisely. Then, Figure 3 confirms the effectiveness of the controller due to a very minute value of the tracking error. Figure 4 presents the control inputs that drive the system state onto and maintain it on the desired surfaces for the desired dynamics, thereby showing the

controller's effort in achieving the tracking. Furthermore, the proposed approach yields smooth control torques. Afterwards, Figure 5 shows the simulations of the adaptive parameters of the proposed and compared schemes. The summary of the collective results, as depicted in Figures 2-5, shows that the APtFoSMC scheme achieves effective position tracking in the presence of unknown uncertain dynamics.

Table 1: Proposed control parameters.

Control parameter	Value
κ ₁	6
κ_2	6
к3	0.0001
κ_4	1
κ ₅	30
κ ₆	30
κ ₇	0.0003
α	0.3
β	0.1
γ	0.1
$x_1(0)$	-0.2
$x_2(0)$	-0.2
$x_3(0)$	-0.2
$\hat{\mathbb{O}}_1(0)$	0.001
$\hat{\mathbb{O}}_2(0)$	0.001
$\hat{\mathbb{O}}_3(0)$	0.001
ρ_1	0.01
ρ_2	0.01
ρ_3	0.01
a	1

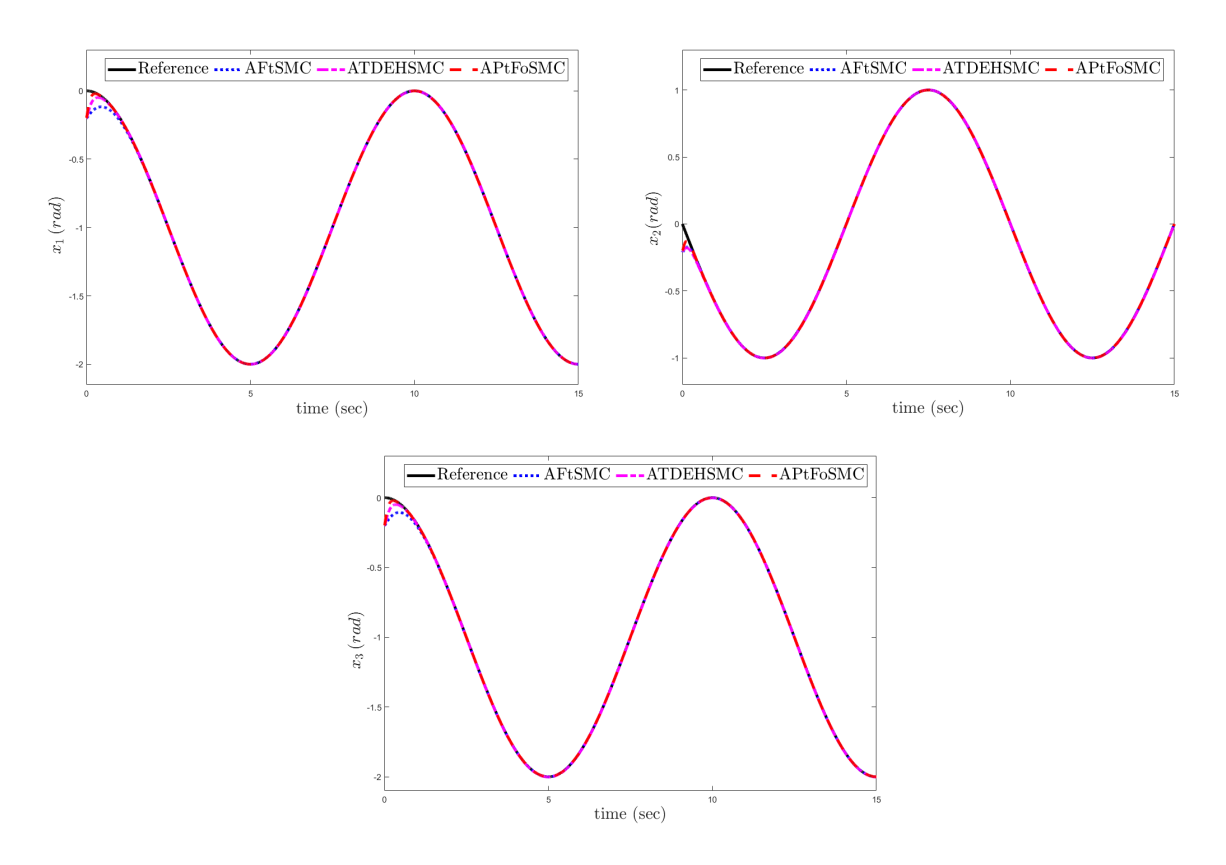


Figure 2: Position tracking under unknown dynamics.

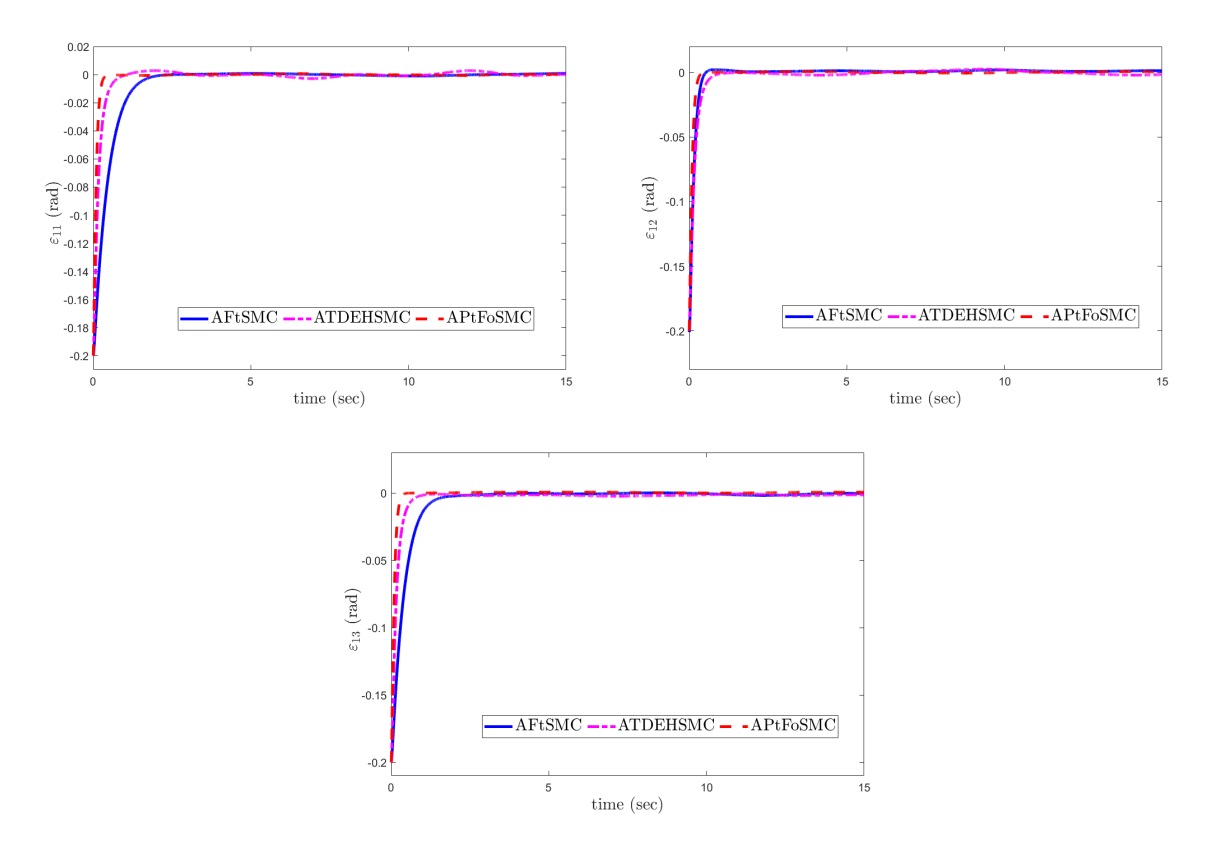


Figure 3: Tracking error under unknown dynamics.

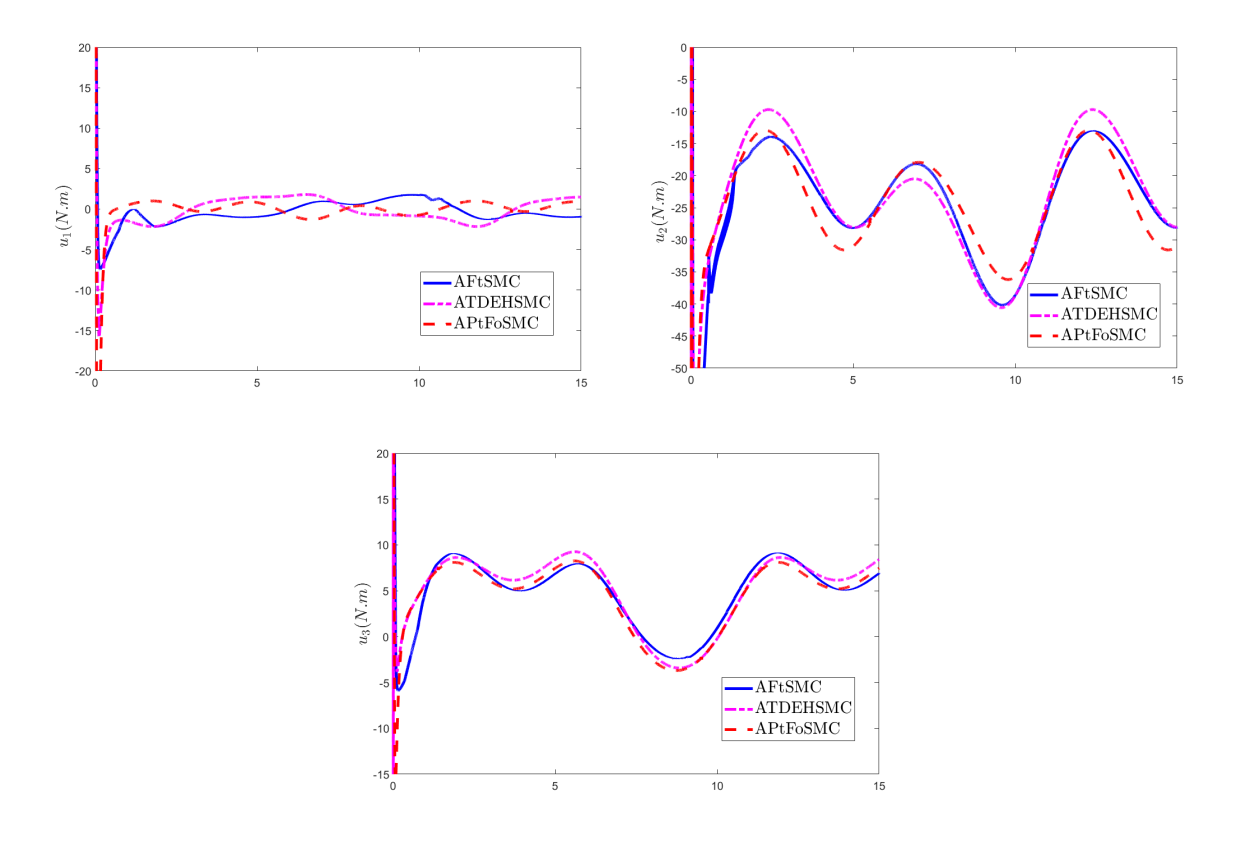


Figure 4: Control input under unknown dynamics.

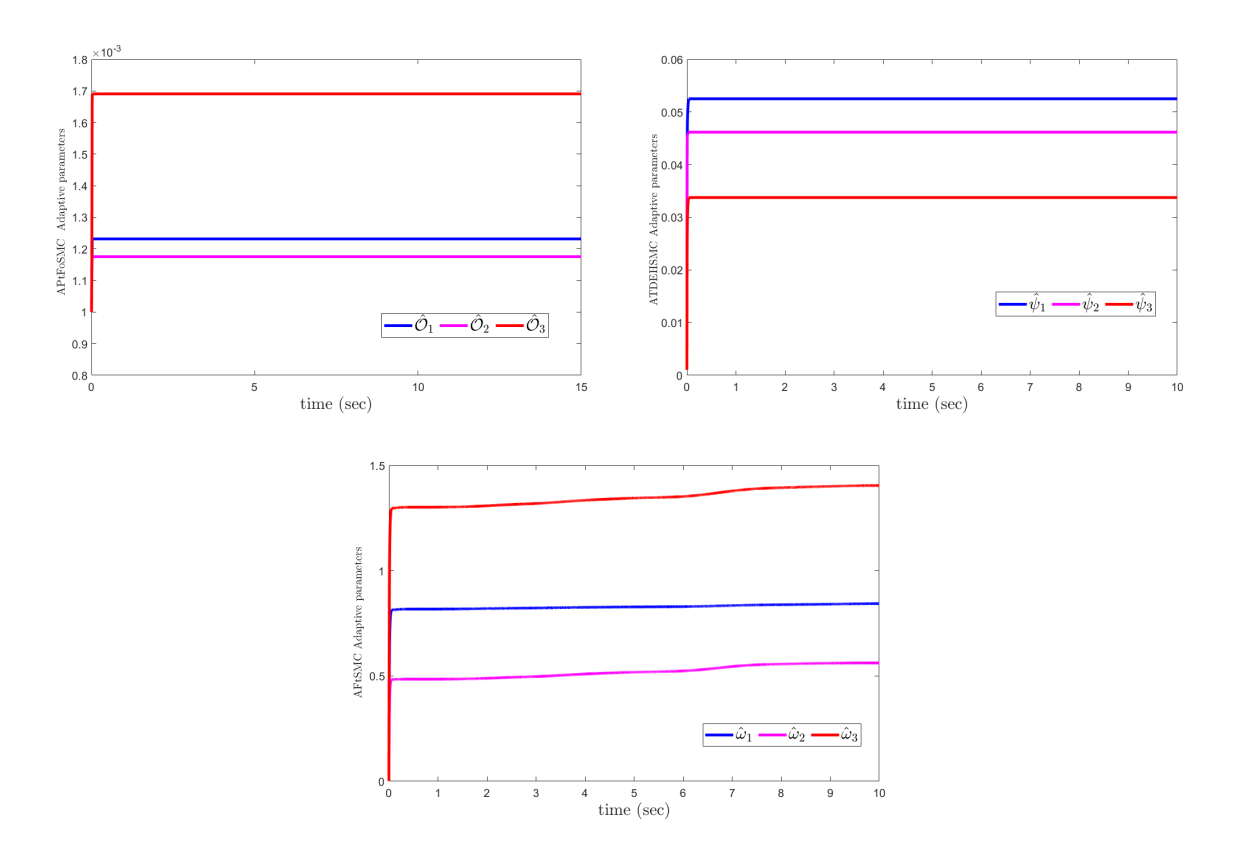


Figure 5: Adaptive gains.

7. Discussion and analysis

We evaluated how well the APtFoSMC scheme performs compared to AFtSMC and ATDEHSMC when dealing with unknown dynamics in Figures 2-5. We focused on how well it tracks position, tracking error, and control torque. Therefore, Figure 2 shows that the APtFoSMC scheme stayed close to the desired path despite uncertainties. This shows it can handle uncertainties and maintain better tracking accuracy than AFtSMC and ATDEHSMC schemes. Moreover, Figure 3 shows that when there are unknown dynamics, the tracking errors for the two schemes are quite different. Compared to AFtSMC and ATDEHSMC, the proposed controller is better at reducing the effect of uncertainties on tracking accuracy. Figure 4 demonstrated that the control torque for APtFoSMC had a small increase in amplitude to preserve tracking precision. However, it stayed within reasonable limits, showing that the controller balanced tracking efficiency and control effort well. Moreover, Figure 5 shows the simulation results for the adaptive parameters used in the suggested scheme and the other comparative schemes. This shows that the proposed scheme has no adaptive parameter drifting.

The simulation results showed that the suggested APtFoSMC scheme works well for accurate tracking control of the joint position with smooth control torque. Compared to AFtSMC and ATDEHSMC, the proposed controller shows notable robustness, even with unknown dynamics. Based on the given range, we chose specific controller parameters to ensure optimal performance: $\kappa_1 > 0$, $\kappa_2 > 0$, $\kappa_3 > 0$, $\kappa_4 > 0$, $\kappa_5 > 0$, $\kappa_6 > 0$, $\kappa_7 > 0$, $\alpha > 0$, $\rho_i > 0$, and $0 < \alpha, \beta, \gamma < 1$. We must carefully choose these parameters to ensure the stability of the closed-loop system. Choosing the wrong parameters can lead to instability. Fortunately, we know the acceptable ranges for each parameter, which makes choosing the right values simpler for the proposed control scheme.

8. Conclusion

The research examines the control of trajectory tracking for robotic manipulators in the presence of uncertainties and external disturbances. An adaptive predefined-time fractional-order sliding mode control scheme is proposed as a solution. APtFoSMC adopts an adaptive mechanism that compensates for the unknown bounds of uncertainties and external disturbances, allowing the system state to converge to the desired trajectory within a predefined time and enhancing tracking performance. The efficacy of the proposed APtFoSMC is confirmed through simulations on a 3-DOF PUMA robot with uncertain dynamics. In comparison, APtfoSMC has a faster convergence, less tracking error, and greater uncertainties and disturbance mitigation compared to AFtSMC and ATDEHSMC controllers. The future work related to the proposed scheme can be extended with learning control methods.

Acknowledgments

This paper is derived from a research grant funded by the Research, Development, and Innovation Authority (RDIA)-Kingdom of Saudi Arabia, with grant number (13382-psu-2023-PSNU-R-3-1-EI-). The authors would like to thank Prince Sultan University, Riyadh, Saudi Arabia, for supporting the article processing charges (APC) of this publication. The authors especially acknowledge the Automated Systems and Computing Lab (ASCL) at Prince Sultan University, Riyadh, Saudi Arabia.

References

- [1] G. E. M. Abro, S. A. B. Zulkifli, V. S. Asirvadam, Z. A. Ali, Model-free-based single-dimension fuzzy SMC design for underactuated quadrotor UAV, Actuators, 10 (2021), 25 pages. 1
- [2] S. Ahmed, A. T. Azar, I. K. Ibraheem, Model-free scheme using time delay estimation with fixed-time FSMC for the nonlinear robot dynamics, AIMS Math., 9 (2024), 9989–10009. 1
- [3] S. Ahmed, A. T. Azar, M. Tounsi, Z. Anjum, Trajectory tracking control of Euler-Lagrange systems using a fractional fixed-time method, Fractals Fract., 7 (2023), 15 pages. 1, 2.2, 3
- [4] S. Ahmed, H. Wang, Y. Tian, Fault tolerant control using fractional-order terminal sliding mode control for robotic manipulators, Stud. Inform. Control, 27 (2018), 55–64. 6
- [5] S. Ahmed, H. Wang, Y. Tian, Adaptive high-order terminal sliding mode control based on time delay estimation for the robotic manipulators with backlash hysteresis, IEEE Trans. Syst. Man Cybern. Syst., 51 (2019), 1128–1137. 6
- [6] A. Ali, K. Shah, T. Abdeljawad, H. Khan, A. Khan, Study of fractional order pantograph type impulsive antiperiodic boundary value problem, Adv. Differ. Equ., 2020 (2020), 32 pages. 1
- [7] A. S. Aljuboury, A. H. Hameed, A. R. Ajel, A. J. Humaidi, A. Alkhayyat, A. K. A. Mhdawi, *Robust adaptive control of knee exoskeleton-assistant system based on nonlinear disturbance observer*, Actuators, **11** (2022), 18 pages. 1
- [8] B. Armstrong, O. Khatib, J. Burdick, *The explicit dynamic model and inertial parameters of the PUMA 560 arm*, In: Proc. IEEE Int. Conf. Robot. Automat., **3** (1986), 510–518. 6
- [9] M. Boukattaya, H. Gassara, Time-varying nonsingular terminal sliding mode control for uncertain second-order nonlinear systems with prespecified time, Int. J. Adapt. Control Signal Process., 36 (2022), 2017–2040. 1
- [10] J. Chen, H. Zhang, Q. Tang, H. Zhang, Adaptive fuzzy sliding mode control of the manipulator based on an improved super-twisting algorithm, Proc. Inst. Mech. Eng. Part C J. Mech. Eng. Sci., 238 (2024), 4294–4306. 1
- [11] J. Chen, C. Zhao, Q. Tang, X. Liu, Z. Wang, C. Tan, J. Wu, T. Long, Low Chattering Trajectory Tracking Control of Non-singular Fast Terminal Sliding Mode Based on Disturbance Observer, Int. J. Control Autom. Syst., 21 (2023), 440–451. 1
- [12] M. S. Elhadidy, W. S. Abdalla, A. A. Abdelrahman, S. Elnaggar, M. Elhosseini, Assessing the accuracy and efficiency of kinematic analysis tools for six-DOF industrial manipulators: the KUKA robot case study, AIMS Math., 9 (2024), 13944–13979. 1
- [13] M. A. Faraj, B. Maalej, N. Derbel, Design and analysis of nonsingular terminal super twisting sliding mode controller for lower limb rehabilitation exoskeleton contacting with ground, Springer, Cham, 491 (2023), 367–386. 1
- [14] M. A. Faraj, B. Maalej, N. Derbel, O. Naifar, Adaptive fractional-order super-twisting sliding mode controller for lower limb rehabilitation exoskeleton in constraint circumstances based on the grey wolf optimization algorithm, Math. Probl. Eng., 2023 (2023), 32 pages. 1
- [15] A. Fekih, S. Mobayen, C. Chen, Adaptive robust fault-tolerant control design for wind turbines subject to pitch actuator faults, Energies, 14 (2021), 13 pages. 1
- [16] Y. Feng, X. Yu, Z. Man, Non-singular terminal sliding mode control of rigid manipulators, Automatica J. IFAC, 38 (2002), 2159–2167. 1

- [17] Z. Han, K. Zhang, T. Yang, M. Zhang, Spacecraft fault-tolerant control using adaptive non-singular fast terminal sliding mode, IET Control Theory Appl., 10 (2016), 1991–1999.
- [18] S. Heidarkhani, A. Salari, Nontrivial solutions for impulsive fractional differential systems through variational methods, Math. Methods Appl. Sci., 43 (2020), 6529–6541. 1
- [19] S. Heidarkhani, A. Salari, G. Caristi, *Infinitely many solutions for impulsive nonlinear fractional boundary value problems*, Adv. Differ. Equ., **2016** (2016), 19 pages. 2.3
- [20] S. Heidarkhani, Y. Zhao, G. Caristi, G. A. Afrouzi, S. Moradi, Infinitely many solutions for perturbed impulsive fractional differential systems, Appl. Anal., 96 (2017), 1401–1424. 1
- [21] A. J. Humaidi, I. K. Ibraheem, A. T. Azar, M. E. Sadiq, A new adaptive synergetic control design for single link robot arm actuated by pneumatic muscles, Entropy, 22 (2020), 24 pages. 1
- [22] P. Ioannou, B. Fidan, Adaptive control tutorial, Society for Industrial and Applied Mathematics (SIAM), Philadel-phia, PA, (2006).
- [23] C. Jing, X. Ma, K. Zhang, Y. Wang, B. Yan, Y. Hui, Actor-Critic Neural-Network-Based Fractional-Order Sliding Mode Control for Attitude Tracking of Spacecraft with Uncertainties and Actuator Faults, Fractal Fract., 8 (2024), 15 pages. 1
- [24] S. B. Joseph, E. G. Dada, A. Abidemi, D. O. Oyewola, B. M. Khammas, *Metaheuristic algorithms for PID controller parameters tuning: Review, approaches and open problems*, Heliyon, 8 (2022), 29 pages. 1
- [25] D. Li, J.-J. E. Slotine, On sliding control for multi-input multi-output nonlinear systems, Am. Control Conf., (1987), 874–879. 1
- [26] N. Mazhar, F. M. Malik, A. Raza, R. Khan, Predefined-time control of nonlinear systems: A sigmoid function based sliding manifold design approach, Alex. Eng. J., 61 (2022), 6831–6841. 1
- [27] A. J. Muñoz-Vázquez, J. D. Sánchez-Torres, S. Gutiérrez-Alcalá, E. Jiménez-Rodríguez, A. G. Loukianov, *Predefined-time robust contour tracking of robotic manipulators*, J. Franklin Inst., **356** (2019), 2709—2722. 1, 2.1
- [28] M. Qin, S. Dian, B. Guo, X. Tao, T. Zhao, Fractional-order SMC controller for mobile robot trajectory tracking under actuator fault, Syst. Sci. Control Eng., 10 (2022), 312–324. 1
- [29] H. Saber, M. A. Almalahi, H. Albala, K. Aldwoah, A. Alsulami, K. Shah, A. Moumen, *Investigating a nonlinear fractional evolution control model using W-piecewise hybrid derivatives: An application of a breast cancer model*, Fractal Fract., 8 (2024), 23 pages. 2.3
- [30] J. G. Sánchez-Torres, D. Gómez-Gutiérrez, E. López, A. G. Loukianov, A class of predefined-time stable dynamical systems, IMA J. Math. Control Inform., 35 (2018), i1–i29. 1
- [31] S. Singh, A. T. Azar, A. Ouannas, Q. Zhu, W. Zhang, J. Na, Sliding mode control technique for multi-switching synchronization of chaotic systems, In: 9th International Conference on Modelling, Identification and Control (ICMIC), IEEE, (2017), 880–885. 1
- [32] S. Souissi, M. Boukattaya, *Time-varying nonsingular terminal sliding mode control of autonomous surface vehicle with predefined convergence time*, Ocean Eng., **263** (2022). 1
- [33] Z. Sun, H. Liu, K. Li, W. Su, Y. Jiang, B. Chen, A Disturbance Observer-Based Fractional-Order Fixed-Time Sliding Mode Control Approach for Elevators, Actuators, 13 (2024), 20 pages. 1
- [34] G. Tao, Multivariable adaptive control: A survey, Automatica J. IFAC, 50 (2014), 2737–2764. 1
- [35] C. Ton, C. Petersen, Continuous fixed-time sliding mode control for spacecraft with flexible appendages, IFAC-PapersOnLine, 51 (2018), 1–5. 1
- [36] Y. Wang, G. Luo, L. Gu, X. Li, Fractional-order nonsingular terminal sliding mode control of hydraulic manipulators using time delay estimation, J. Vib. Control, 22 (2016), 3998–4011. 1
- [37] H. Xue, X. Liu, A novel fast terminal sliding mode with predefined-time synchronization, Chaos Solitons Fractals, 175 (2023), 13 pages. 1
- [38] L. Yang, J. Yang, Nonsingular fast terminal sliding-mode control for nonlinear dynamical systems, Int. J. Robust Nonlinear Control, 21 (2011), 1865–1879.
- [39] C. Yin, X. Huang, Y. Chen, S. Dadras, S.-M. Zhong, Y. Cheng, Fractional-order exponential switching technique to enhance sliding mode control, Appl. Math. Model., 44 (2017), 705–726. 2.4
- [40] I. Zaway, R. Jallouli-Khlif, B. Maalej, H. Medhaffar, N. Derbel, From PD to Fractional Order PD controller used for gait rehabilitation, 18th Int. Multi-Conf. Syst. Signals Devices, (2021), 948–953. 1
- [41] Y. Zhang, M. Chadli, Z. Xiang, Predefined-time adaptive fuzzy control for a class of nonlinear systems with output hysteresis, IEEE Trans. Fuzzy Syst., 31 (2022), 2522–2531. 1
- [42] D. Zhao, S. Li, F. Gao, A new terminal sliding mode control for robotic manipulators, IFAC Proc. Vol., 41 (2008), 9888–9893. 1